PROCEEDINGS OF SCIENCE

Depth of Maximum of Air-Shower Profiles above $10^{17.8}$ eV Measured with the Fluorescence Detector of the Pierre Auger Observatory and Mass-Composition Implications

Thomas Fitoussi[a,*] **for the Pierre Auger Collaboration**[b]

[a] *Karlsruhe Institute of Technology KIT, Institute for Astroparticle Physics, Karlsruhe, Germany*

[b] *Observatorio Pierre Auger, Av. San Martín Norte 304, 5613 Malargüe, Argentina*

Full author list: https://www.auger.org/archive/authors_icrc_2023.html

E-mail: spokespersons@auger.org

After seventeen years of operation, the first phase of measurements at the Pierre Auger Observatory finished and the process of upgrading it began. In this work, we present distributions of the depth of air-shower maximum, $X_{\rm max}$, using profiles measured with the fluorescence detector of the Pierre Auger Observatory. The analysis is based on the Phase I data collected from 01 December 2004 to 31 December 2021.

The $X_{\rm max}$ measurements take advantage of an improved evaluation of the vertical aerosol optical depth and reconstruction of the shower profiles. We present the energy dependence of the mean and standard deviation of the $X_{\rm max}$ distributions above $10^{17.8}$ eV. Both $X_{\rm max}$ moments are corrected for detector effects and interpreted in terms of the mean logarithmic mass and variance of the masses by comparing them to the predictions of post-LHC hadronic interaction models. We corroborate our earlier findings regarding the change of the elongation rate of the mean $X_{\rm max}$ at $10^{18.3}$ eV with higher significance. We also confirm, with four more years of data compared to the last results presented in 2019, that around the ankle in the cosmic rays spectrum, the proton component gradually disappears and that intermediate mass nuclei dominate the composition at ultra-high energies.

The 38th International Cosmic Ray Conference (ICRC 2023)
July 6th – August 3rd, 2023
Nagoya, Japan

*Speaker

PoS(ICRC2023)319

1. Introduction

The mass composition of Ultra-High Energy Cosmic Rays (UHECRs) is a key feature to identify their sources and constrain the astrophysical processes of their production (see e.g. Ref. [1]). A change in the elongation rate around the ankle (~4 EeV) has been shown. It could be explained by the transition between the Galactic and extragalactic origin or two extragalactic components. Meanwhile the composition at the suppression (>30 EeV) is uncertain due to the lack of statistics [2–5].

Inferring the composition of UHECRs is a complex task. The measurement of the depth of maximum $X_{\rm max}$ of the air-shower profile is still the main proxy for the mass composition. The fluorescence light emitted by the de-excitation of nitrogen molecules when air-showers pass through the atmosphere can be observed by the fluorescence detector (FD) of the Pierre Auger Observatory, consisting of twenty-seven telescopes located on four sites surrounding the 3000 km^2 surface detector array (SD). On each site, the shower profile is reconstructed by six fluorescence telescopes to determine its depth of maximum $X_{\rm max}$. Due to shower-to-shower fluctuations, individual determination of the mass of a particular cosmic ray is impossible but the energy dependency of the mean and standard deviation of the $X_{\rm max}$ distributions can be interpreted with different hadronic models [6–8] to infer the composition of UHECRs.

The Pierre Auger Observatory began taking data in 2004. In 2020, the deployment of the upgrade of the surface detector started, ending Phase I of the observatory. In 2014, the Pierre Auger Observatory published the first results of the mass composition [2, 3] and these results has been updated regularly since [4, 5]. Recently the atmosphere attenuation measurements at the Pierre Auger Observatory have been improved [9] as well as the reconstruction of the longitudinal shower profiles [10]. In this proceeding, taking advantage of these improvements, the new $X_{\rm max}$ moments are measured and the interpretation with the post-LHC hadronic models are presented for the full Phase I data, extending from 01 December 2004 to 31 December 2021.

2. Data analysis

At the Pierre Auger Observatory, the fluorescence light is measured by 24 "standard" telescopes that cover 30° in azimuth and between 1.5 and 30° in elevation located on four sites surrounding the 3000 km^2 surface detector array. Three additional telescopes (HEAT) looking at higher elevation (30° to 58°) have been operating at the Cohihueco site since 2009, allowing for the detection of air showers below 10^{18} eV. This proceeding will only focus on the analysis of the data from the "standard" telescopes for showers with energy above $10^{17.8}$ eV.

2.1 Data selection

The data selection in this proceeding is based on the one used in Ref. [2]. To ensure a selection of good quality events with an accurate reconstruction of the $X_{\rm max}$ and the energy of the shower, the pressure, the humidity and the temperature as well as the presence of clouds are monitored with multiple instruments. Importantly, vertical aerosol optical depth (VAOD) measurements have been updated [9]. Good atmospheric conditions are ensured by imposing the VAOD to be lower than 0.1 up to 3 km above ground and that there is no cloud that can affect the reconstruction.

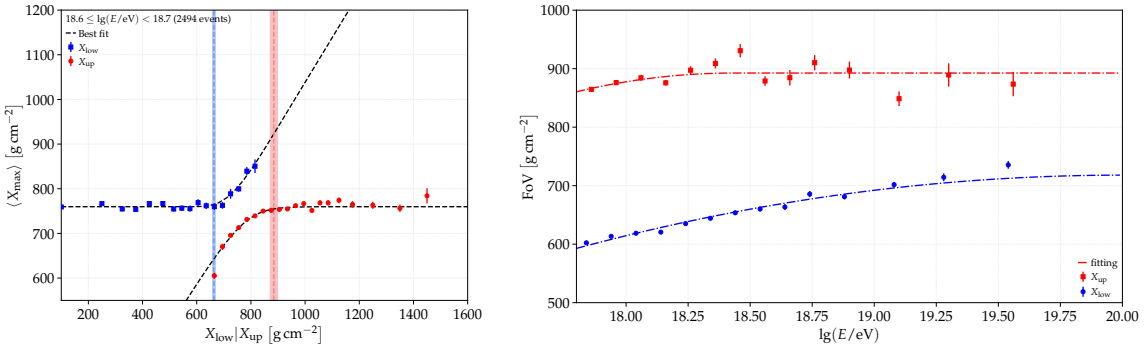

Figure 1: *Left:* $\langle X_{\rm max}\rangle$ versus $X_{\rm low}$ and $X_{\rm up}$ for events between $10^{18.6}$ and $10^{18.7}$ eV with the corresponding cuts. *Right:* $X_{\rm low}^{\rm cut}$ and $X_{\rm up}^{\rm cut}$ cuts versus energy. See text for more information.

Only hybrid events are considered. These are events where the geometry is reconstructed using both the arrival time of ultra-violet light in the fluorescence telescopes and the timing of the closest surface detector station to the shower core. The reconstruction of the shower profiles with the FD has been updated and improved [10]. In addition to fiducial field of view selection criteria, showers are selected if $X_{\rm max}$ is inside the geometrical field of view of the telescope, if the $X_{\rm max}$ reconstruction uncertainty is below 40 g/cm^2 and if the Cherenkov light contamination is smaller than 20%.

2.2 Fiducial field of view cuts

The selection of good quality showers may introduce an $X_{\rm max}$ selection bias (i.e. showers with $X_{\rm max}$ values within certain range are more likely to be of good quality), which will bias the reconstructed $X_{\rm max}$ distribution. In order to avoid this bias, we apply a fiducial field of view cut. For each energy bin, an upper and a lower bound for a slant depth range is computed ($X_{\rm up}^{\rm cut}$, $X_{\rm low}^{\rm cut}$). The key to sample an unbiased $X_{\rm max}$ distribution is to have the boundaries $X_{\rm up}^{\rm cut}$, $X_{\rm low}^{\rm cut}$ encompassing the true $X_{\rm max}$ distribution for the corresponding energy bin.

In order to determine the $X_{\rm up}^{\rm cut}$, $X_{\rm low}^{\rm cut}$ for each energy bin, the mean of the $X_{\rm max}$ distribution $\langle X_{\rm max}\rangle$ is computed for binned $X_{\rm low}$ and $X_{\rm up}$ (respectively blue and red points in Fig. 1–left). The values $X_{\rm low}$ and $X_{\rm up}$ define the slant depth range where the corresponding event could have its $X_{\rm max}$ reconstructed reliably. If we allow $X_{\rm low}$ values that are too high or allow $X_{\rm up}$ values too low, then the mean $\langle X_{\rm max}\rangle$ will deviate from its true value (i.e. the $X_{\rm max}$ distribution would be truncated). The obtained truncated-means can be fitted together (black dashed line in Fig. 1-left). Finally, the limits on $X_{\rm up}$ and $X_{\rm low}$ ($X_{\rm low}^{\rm cut}$, $X_{\rm up}^{\rm cut}$) are obtained by determining the depth at which $\langle X_{\rm max}\rangle$ deviates from the asymptotic value by more than $\Delta = 5$ g/cm^2 (blue and red vertical lines in Fig. 1–left). Errors on the cuts are computed by propagating the error on the fitting of the truncated $\langle X_{\rm max}\rangle$. The results of the cuts for all energy bins are displayed in Fig. 1–right (respectively blue for $X_{\rm low}^{\rm cut}$ and red for $X_{\rm up}^{\rm cut}$). $X_{\rm low}^{\rm cut}$ and $X_{\rm up}^{\rm cut}$ are fitted versus the logarithm of the energy separately with the same function as in Ref. [2] (blue and red dotted dashed lines). The $X_{\rm up}$ cut remains the same but the $X_{\rm low}^{\rm cut}$ cuts has increased by ~20 g/cm^2 due to the improvement of the shower profile reconstruction [10]. Events are selected if they have $X_{\rm low} \leqslant X_{\rm low}^{\rm cut}$ and $X_{\rm up} \geqslant X_{\rm up}^{\rm cut}$. This change in $X_{\rm low}^{\rm cut}$ allows for an increase of the number of events selected from ~27% events passing the cut in Ref. [5] to ~29%.

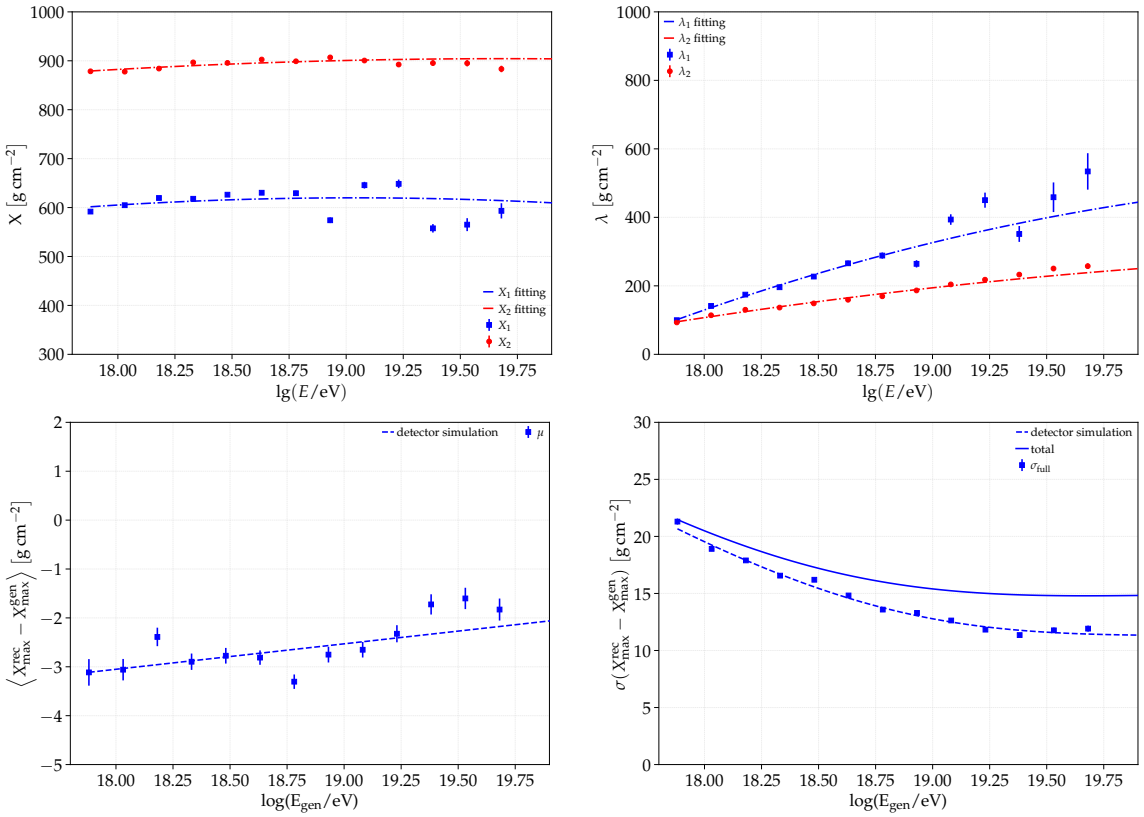

Figure 2: *Top:* Energy dependency of acceptance parameters X_1, X_2, λ_1 and λ_2. *Bottom:* from left to right, energy dependency of $X_{\max}$ bias and resolution. See text for more information.

2.3 Detector effects

Once good quality events are selected and the fiducial field of view cuts are applied, the detector response has to be taken into account to correct small residual biases in the $X_{\max}$ distributions. This correction includes the combined efficiencies for event trigger, event reconstruction and event selection (referred to as "acceptance") as a function of $X_{\max}$. Furthermore, the reconstruction biases in energy and $X_{\max}$ and the average $X_{\max}$ resolution for each energy bin are calculated using detector simulations. To compute the $X_{\max}$ acceptance, we generated air showers with CONEX [11] using the Sybill2.3d [8] hadronic model for protons and iron nuclei with a flat $X_{\max}$ distribution injection. The simulation of the atmosphere and the detector response and reconstruction are made with the Auger Offline software [12] to take into account the real-time state for the SD and FD [13].

After applying the same selection as applied to real data, the efficiency ε (i.e. $X_{\max}$ acceptance) in each energy bin can be modeled by four parameters X_1, X_2, λ_1 and λ_2 defined by

$$\varepsilon = \begin{cases} e^{(X_{\max}-X_1)/\lambda_1} & \text{if } X_{\max} < X_1 \\ e^{-(X_{\max}-X_2)/\lambda_2} & \text{if } X_{\max} > X_2 \\ \text{const.} & \text{otherwise} \end{cases} \quad (1)$$

The energy dependency of these parameters is presented in the top panels of Fig. 2. They show the

results from simulations (points) and the parametrization used for correction. Results are equivalent as the one previously published [4].

Regarding the reconstruction biases in energy and $X_{\rm max}$ and the $X_{\rm max}$ resolution. We simulated $X_{\rm max}$ distributions similar to the observed ones (i.e. mixed composition) and passed through the detector simulation, event reconstruction and event selection procedures, in the same way as with real data. This way the end-to-end residual biases and $X_{\rm max}$ resolution are calculated. For example, the $X_{\rm max}$ bias is defined as $X_{\rm max}^{\rm bias} = X_{\rm max}^{\rm rec} - X_{\rm max}^{\rm gen}$. The bottom panels in Fig. 2 show the $X_{\rm max}$ bias (on the left) and the $X_{\rm max}$ resolution (on the right). They correspond to the mean and the standard deviation of $X_{\rm max}^{\rm bias}$ respectively as function of the energy. The bias decreases as the energy increases but remains between -3 and -1 g/cm^2 while the standard deviation is also decreasing with energy from 22 to 12 g/cm^2 (dashed line). The total $X_{\rm max}$ resolution is represented on Fig. 2 (bottom, right) by the plain line. It includes uncorrelated uncertainties from the atmosphere (precision of aerosols, molecular atmosphere) and alignment of the telescopes, see [2]. The systematic uncertainties of the $X_{\rm max}$ scale and resolution remain unchanged from Ref. [2] apart from the VAOD uncertainties which have been updated [9].

3. Results

The raw $X_{\rm max}$ distributions after quality and fiducial field of view cuts are shown in Fig. 6. A total of 75 210 events passed all the selections. Compared to Ref. [5] it is an increase of 60%. This significant augmentation has three reasons: four more years of data, the improvement of the fiducial field of view cut (see Sec. 2.2) and the adding of the events observed by the Cohihueco site, that were previously merged in the HEAT / Cohihueco dataset [4] (for energies below $10^{18.1}$ eV). The last point contributes to increase the number of events at low energy. Above 10^{19} eV, the number of events has increases by 26%. These distributions are used to fit the composition fraction of protons, helium, nitrogen and iron (see Ref. [14]). In this proceeding we will only focus on the moments of $X_{\rm max}$ and $\ln A$. For this purpose, the $X_{\rm max}$ and energy bias, estimated in the previous section are corrected for each event. Then, $X_{\rm max}$ moments are estimated from the distributions (Fig. 6), where the $X_{\rm max}$ acceptance is taken into account using the Λ_η method described in Ref. [2]. Finally, the $X_{\rm max}$ resolution is subtracted in quadrature from the computed $\sigma(X_{\rm max})$ values.

The moments obtained are represented in Fig. 3. With the new aerosol measurements increasing the aerosol attenuation [9], the $\langle X_{\rm max}\rangle$ has increased by 1 to 4 g/cm^2 compared to Ref. [2]. Despite this small change, the results previously observed by the Pierre Auger Observatory [2, 4, 5] are confirmed: a break in the composition evolution at $\sim 10^{18.4}$ eV illustrated in Fig. 4 by a linear fit with one break (green dashed line). The $\langle X_{\rm max}\rangle$ elongation rate fitted before the break is ~ 81 g/cm^2 / decade while after the break it is ~ 28 (g/cm^2) / decade. This change in the elongation rate argues for a composition becoming lighter from $10^{17.8}$ to $10^{18.3}$ eV before becoming heavier as the energy increases. At the same time, the change of slope of the $\sigma(X_{\rm max})$ evolution indicates a mixed composition below $10^{18.3}$ eV and a purer composition at higher energy.

The $X_{\rm max}$ moments can be converted [2] to a mean and variance of the logarithm of the mass

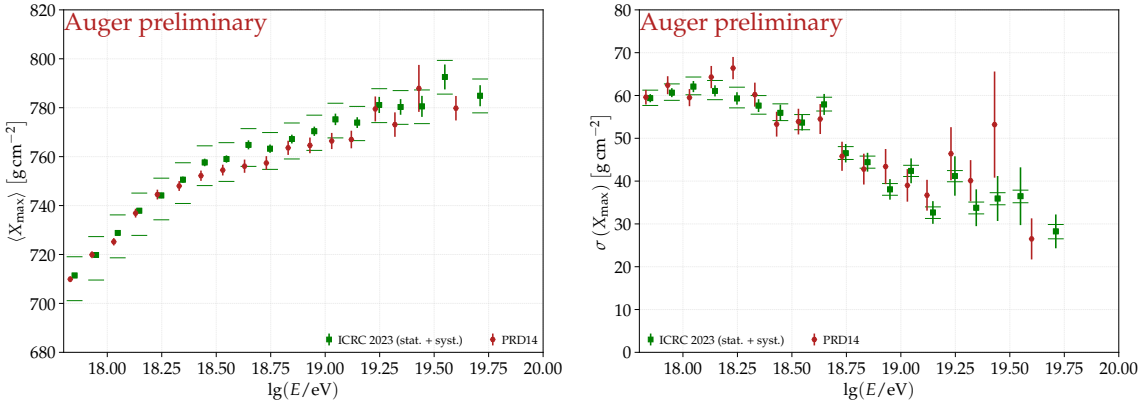

Figure 3: Mean $\langle X_{\rm max} \rangle$ and $\sigma(X_{\rm max})$ of the $X_{\rm max}$ distributions versus energy from this proceeding compared with the one obtained in Ref. [2].

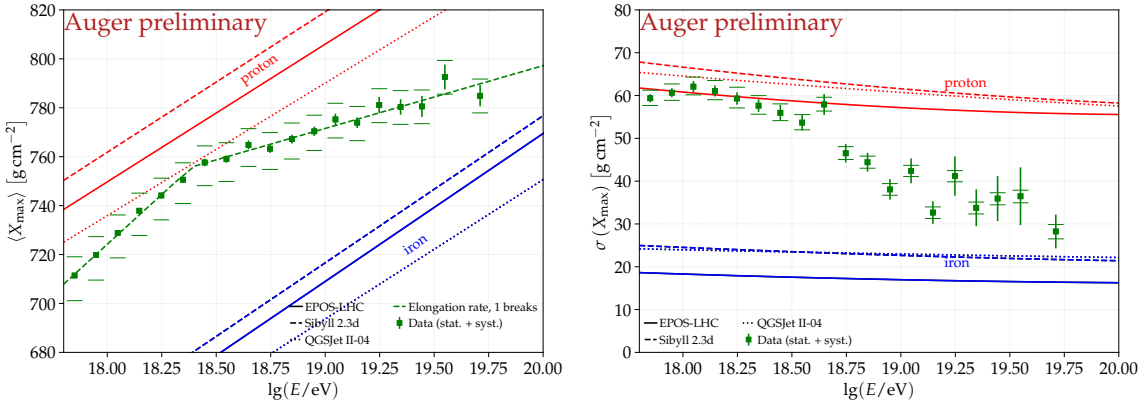

Figure 4: Mean $\langle X_{\rm max} \rangle$ and $\sigma(X_{\rm max})$ of the $X_{\rm max}$ distributions versus energy with elongation rate fitting. As comparison predictions from hadronic models [6–8] are also displayed.

number ln A by using

$$\langle X_{\rm max} \rangle = \langle X_{\rm max} \rangle_{\rm p} + f_E \langle \ln A \rangle \tag{2}$$

$$\sigma^2(X_{\rm max}) = \langle \sigma^2_{\rm sh} \rangle + f_E^2 \, \sigma^2(\ln A) \tag{3}$$

where $\langle X_{\rm max} \rangle_{\rm p}$ is the mean $X_{\rm max}$ for protons, $\sigma^2_{\rm sh}$ is the average shower-to-shower fluctuations and f_E is an energy-dependent parameter. All three are parametrized for different hadronic models. The results for three different hadronic models, QGSJetII-04 [6], EPOS-LHC [7] and Sybill2.3d [8], are shown in Fig. 5. As can be seen, the interpretation with QGSJetII-04 results into negative values for $\sigma^2(\ln A)$ which is nonphysical. For the other two models, we corroborate our previous findings of a $\sigma^2(\ln A)$ close to zero, i.e. a less mixed cosmic-ray composition arrives at Earth above 10^{19} eV.

References

[1] A. Coleman et al., *Astropart. Phys.* **149** (2023) 102819.
[2] A. Aab et al., [Pierre Auger Coll.], *Phys. Rev. D* **90** (2014) 122005.
[3] A. Aab et al., [Pierre Auger Coll.], *Phys. Rev. D* **90** (2014) 122006.

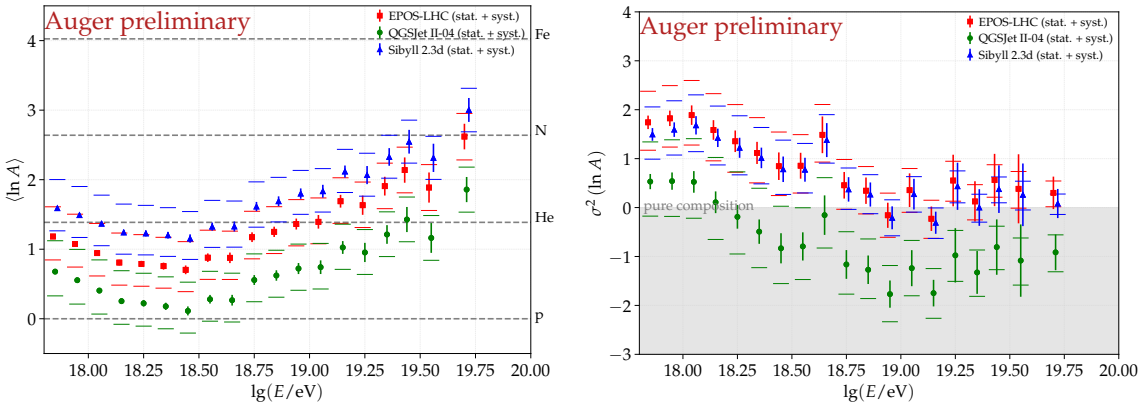

Figure 5: Mean and variance of the logarithm of the mass number ln A for different hadronic models.

[4] J. Bellido, [Pierre Auger Coll.], *EPJ Web Conf.* **301** (2018) 506.
[5] A. Yushkov, [Pierre Auger Coll.], *EPJ Web Conf.* **358** (2021) 482.
[6] S. Ostapchenko, *Phys. Rev. D* **81** (2010) 114028.
[7] T. Pierog et al., *Phys. Rev. C* **92** (2015) 034906.
[8] F. Riehn et al., *Phys. Rev. D* **102** (2020) 063002.
[9] V.M. Harvey, [Pierre Auger Coll.], *EPJ Web Conf.* **444** (2023) 300.
[10] J. Bellido, [Pierre Auger Coll.], *EPJ Web Conf.* **444** (2023) 211.
[11] T. Bergmann et al., *Astropart. Phys.* **26** (2007) 063002.
[12] S. Argiro et al., *Nucl. Instrum. Methods Phys. Res.* **580** (2007) 1485.
[13] P. Abreu et al., [Pierre Auger Coll.], *Astropart. Phys.* **34** (2011) 368.
[14] O. Tkachenko, [Pierre Auger Coll.], *EPJ Web Conf.* **444** (2023) 438.

PoS(ICRC2023)319

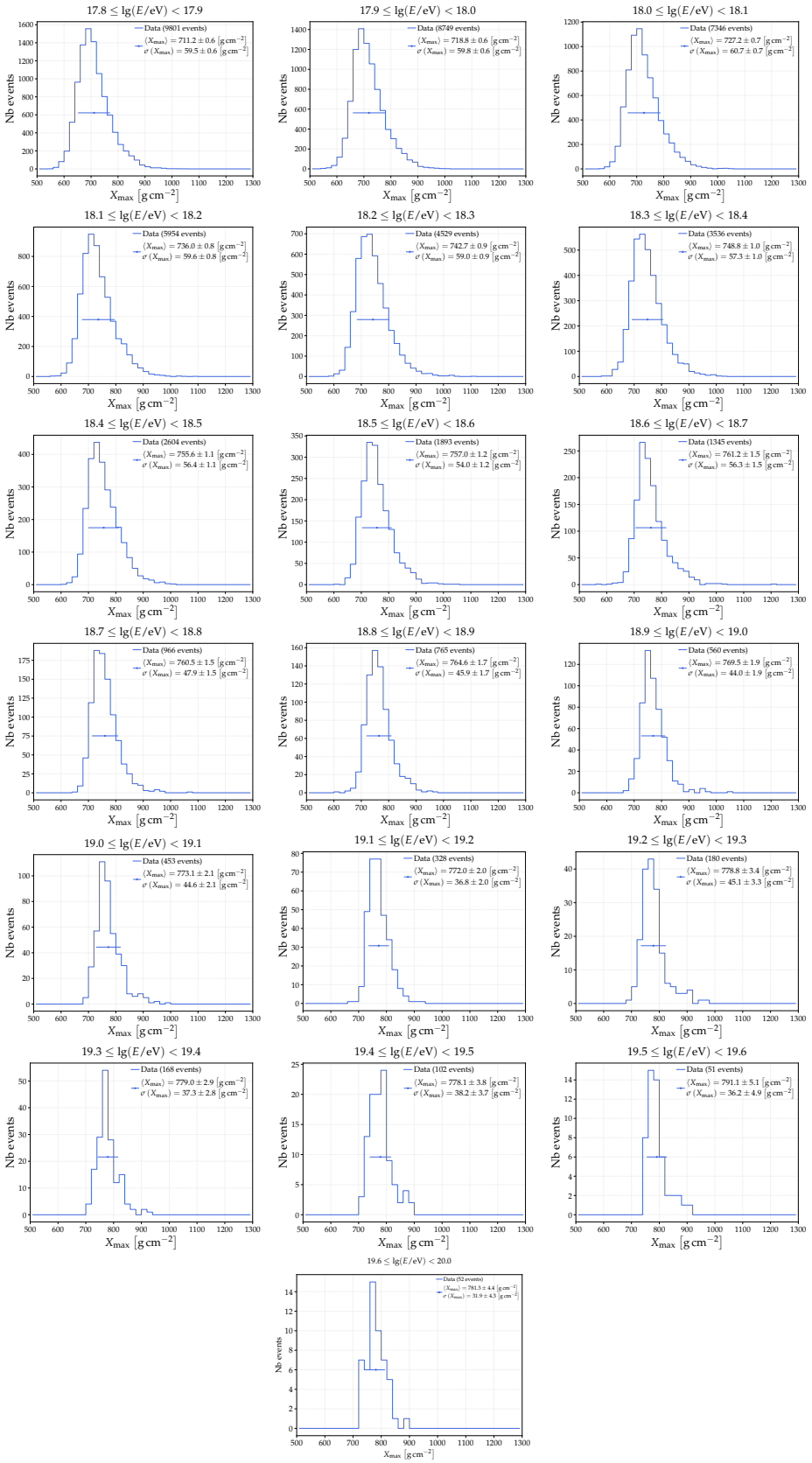

Figure 6: X_{max} distributions for energy bins from $10^{17.8}$ to 10^{20} eV.

The Pierre Auger Collaboration

A. Abdul Halim[13], P. Abreu[72], M. Aglietta[54,52], I. Allekotte[1], K. Almeida Cheminant[70], A. Almela[7,12], R. Aloisio[45,46], J. Alvarez-Muñiz[79], J. Ammerman Yebra[79], G.A. Anastasi[54,52], L. Anchordoqui[86], B. Andrada[7], S. Andringa[72], C. Aramo[50], P.R. Araújo Ferreira[42], E. Arnone[63,52], J. C. Arteaga Velázquez[67], H. Asorey[7], P. Assis[72], G. Avila[11], E. Avocone[57,46], A.M. Badescu[75], A. Bakalova[32], A. Balaceanu[73], F. Barbato[45,46], A. Bartz Mocellin[85], J.A. Bellido[13,69], C. Berat[36], M.E. Bertaina[63,52], G. Bhatta[70], M. Bianciotto[63,52], P.L. Biermann[h], V. Binet[5], K. Bismark[39,7], T. Bister[80,81], J. Biteau[37], J. Blazek[32], C. Bleve[36], J. Blümer[41], M. Boháčová[32], D. Boncioli[57,46], C. Bonifazi[8,26], L. Bonneau Arbeletche[21], N. Borodai[70], J. Brack[j], P.G. Brichetto Orchera[7], F.L. Briechle[42], A. Bueno[78], S. Buitink[15], M. Buscemi[47,61], M. Büsken[39,7], A. Bwembya[80,81], K.S. Caballero-Mora[66], S. Cabana-Freire[79], L. Caccianiga[59,49], I. Caracas[38], R. Caruso[58,47], A. Castellina[54,52], F. Catalani[18], G. Cataldi[48], L. Cazon[79], M. Cerda[10], A. Cermenati[45,46], J.A. Chinellato[21], J. Chudoba[32], L. Chytka[33], R.W. Clay[13], A.C. Cobos Cerutti[6], R. Colalillo[60,50], A. Coleman[90], M.R. Coluccia[48], R. Conceição[72], A. Condorelli[37], G. Consolati[49,55], M. Conte[56,48], F. Convenga[41], D. Correia dos Santos[28], P.J. Costa[72], C.E. Covault[84], M. Cristinziani[44], C.S. Cruz Sanchez[3], S. Dasso[4,2], K. Daumiller[41], B.R. Dawson[13], R.M. de Almeida[28], J. de Jesús[7,41], S.J. de Jong[80,81], J.R.T. de Mello Neto[26,27], I. De Mitri[45,46], J. de Oliveira[17], D. de Oliveira Franco[21], F. de Palma[56,48], V. de Souza[19], E. De Vito[56,48], A. Del Popolo[58,47], O. Deligny[34], N. Denner[32], L. Deval[41,7], A. di Matteo[52], M. Dobre[73], C. Dobrigkeit[21], J.C. D'Olivo[68], L.M. Domingues Mendes[72], J.C. dos Anjos, R.C. dos Anjos[25], J. Ebr[32], F. Ellwanger[41], M. Emam[80,81], R. Engel[39,41], I. Epicoco[56,48], M. Erdmann[42], A. Etchegoyen[7,12], C. Evoli[45,46], H. Falcke[80,82,81], J. Farmer[89], G. Farrar[88], A.C. Fauth[21], N. Fazzini[e], F. Feldbusch[40], F. Fenu[41,d], A. Fernandes[72], B. Fick[87], J.M. Figueira[7], A. Filipčič[77,76], T. Fitoussi[41], B. Flaggs[90], T. Fodran[80], T. Fujii[89,f], A. Fuster[7,12], C. Galea[80], C. Galelli[59,49], B. García[6], C. Gaudu[38], H. Gemmeke[40], F. Gesualdi[7,41], A. Gherghel-Lascu[73], P.L. Ghia[34], U. Giaccari[48], M. Giammarchi[49], J. Glombitza[42,g], F. Gobbi[10], F. Gollan[7], G. Golup[1], M. Gómez Berisso[1], P.F. Gómez Vitale[11], J.P. Gongora[11], J.M. González[1], N. González[7], I. Goos[1], D. Góra[70], A. Gorgi[54,52], M. Gottowik[79], T.D. Grubb[13], F. Guarino[60,50], G.P. Guedes[22], E. Guido[44], S. Hahn[39], P. Hamal[32], M.R. Hampel[7], P. Hansen[3], D. Harari[1], V.M. Harvey[13], A. Haungs[41], T. Hebbeker[42], C. Hojvat[e], J.R. Hörandel[80,81], P. Horvath[33], M. Hrabovský[33], T. Huege[41,15], A. Insolia[58,47], P.G. Isar[74], P. Janecek[32], J.A. Johnsen[85], J. Jurysek[32], A. Kääpä[38], K.H. Kampert[38], B. Keilhauer[41], A. Khakurdikar[80], V.V. Kizakke Covilakam[7,41], H.O. Klages[41], M. Kleifges[40], F. Knapp[39], N. Kunka[40], B.L. Lago[16], N. Langner[42], M.A. Leigui de Oliveira[24], Y Lema-Capeans[79], V. Lenok[39], A. Letessier-Selvon[35], I. Lhenry-Yvon[34], D. Lo Presti[58,47], L. Lopes[72], L. Lu[91], Q. Luce[39], J.P. Lundquist[76], A. Machado Payeras[21], M. Majercakova[32], D. Mandat[32], B.C. Manning[13], P. Mantsch[e], S. Marafico[34], F.M. Mariani[59,49], A.G. Mariazzi[3], I.C. Mariş[14], G. Marsella[61,47], D. Martello[56,48], S. Martinelli[41,7], O. Martínez Bravo[64], M.A. Martins[79], M. Mastrodicasa[57,46], H.J. Mathes[41], J. Matthews[a], G. Matthiae[62,51], E. Mayotte[85,38], S. Mayotte[85], P.O. Mazur[e], G. Medina-Tanco[68], J. Meinert[38], D. Melo[7], A. Menshikov[40], C. Merx[41], S. Michal[33], M.I. Micheletti[5], L. Miramonti[59,49], S. Mollerach[1], F. Montanet[36], L. Morejon[38], C. Morello[54,52], A.L. Müller[32], K. Mulrey[80,81], R. Mussa[52], M. Muzio[88], W.M. Namasaka[38], S. Negi[32], L. Nellen[68], K. Nguyen[87], G. Nicora[9], M. Niculescu-Oglinzanu[73], M. Niechciol[44], D. Nitz[87], D. Nosek[31], V. Novotny[31], L. Nožka[33], A Nucita[56,48], L.A. Núñez[30], C. Oliveira[19], M. Palatka[32], J. Pallotta[9], S. Panja[32], G. Parente[79], T. Paulsen[38], J. Pawlowsky[38], M. Pech[32], J. Pękala[70], R. Pelayo[65], L.A.S. Pereira[23], E.E. Pereira Martins[39,7], J. Perez Armand[20], C. Pérez Bertolli[7,41], L. Perrone[56,48], S. Petrera[45,46], C. Petrucci[57,46], T. Pierog[41], M. Pimenta[72], M. Platino[7], B. Pont[80], M. Pothast[81,80], M. Pourmohammad Shahvar[61,47], P. Privitera[89], M. Prouza[32], A. Puyleart[87], S. Querchfeld[38], J. Rautenberg[38], D. Ravignani[7], M. Reininghaus[39], J. Ridky[32], F. Riehn[79], M. Risse[44], V. Rizi[57,46], W. Rodrigues de Carvalho[80], E. Rodriguez[7,41], J. Rodriguez Rojo[11], M.J. Roncoroni[7], S. Rossoni[43], M. Roth[41], E. Roulet[1], A.C. Rovero[4], P. Ruehl[44], A. Saftoiu[73], M. Saharan[80], F. Salamida[57,46], H. Salazar[64], G. Salina[51], J.D. Sanabria Gomez[30], F. Sánchez[7], E.M. Santos[20], E. Santos[32],

F. Sarazin[85], R. Sarmento[72], R. Sato[11], P. Savina[91], C.M. Schäfer[41], V. Scherini[56,48], H. Schieler[41], M. Schimassek[34], M. Schimp[38], F. Schlüter[41], D. Schmidt[39], O. Scholten[15,i], H. Schoorlemmer[80,81], P. Schovánek[32], F.G. Schröder[90,41], J. Schulte[42], T. Schulz[41], S.J. Sciutto[3], M. Scornavacche[7,41], A. Segreto[53,47], S. Sehgal[38], S.U. Shivashankara[76], G. Sigl[43], G. Silli[7], O. Sima[73,b], F. Simon[40], R. Smau[73], R. Šmída[89], P. Sommers[k], J.F. Soriano[86], R. Squartini[10], M. Stadelmaier[32], D. Stanca[73], S. Stanič[76], J. Stasielak[70], P. Stassi[36], S. Strähnz[39], M. Straub[42], M. Suárez-Durán[14], T. Suomijärvi[37], A.D. Supanitsky[7], Z. Svozilikova[32], Z. Szadkowski[71], A. Tapia[29], C. Taricco[63,52], C. Timmermans[81,80], O. Tkachenko[41], P. Tobiska[32], C.J. Todero Peixoto[18], B. Tomé[72], Z. Torrès[36], A. Travaini[10], P. Travnicek[32], C. Trimarelli[57,46], M. Tueros[3], M. Unger[41], L. Vaclavek[33], M. Vacula[33], J.F. Valdés Galicia[68], L. Valore[60,50], E. Varela[64], A. Vásquez-Ramírez[30], D. Veberič[41], C. Ventura[27], I.D. Vergara Quispe[3], V. Verzi[51], J. Vicha[32], J. Vink[83], J. Vlastimil[32], S. Vorobiov[76], C. Watanabe[26], A.A. Watson[c], A. Weindl[41], L. Wiencke[85], H. Wilczyński[70], D. Wittkowski[38], B. Wundheiler[7], B. Yue[38], A. Yushkov[32], O. Zapparrata[14], E. Zas[79], D. Zavrtanik[76,77], M. Zavrtanik[77,76]

[1] Centro Atómico Bariloche and Instituto Balseiro (CNEA-UNCuyo-CONICET), San Carlos de Bariloche, Argentina
[2] Departamento de Física and Departamento de Ciencias de la Atmósfera y los Océanos, FCEyN, Universidad de Buenos Aires and CONICET, Buenos Aires, Argentina
[3] IFLP, Universidad Nacional de La Plata and CONICET, La Plata, Argentina
[4] Instituto de Astronomía y Física del Espacio (IAFE, CONICET-UBA), Buenos Aires, Argentina
[5] Instituto de Física de Rosario (IFIR) – CONICET/U.N.R. and Facultad de Ciencias Bioquímicas y Farmacéuticas U.N.R., Rosario, Argentina
[6] Instituto de Tecnologías en Detección y Astropartículas (CNEA, CONICET, UNSAM), and Universidad Tecnológica Nacional – Facultad Regional Mendoza (CONICET/CNEA), Mendoza, Argentina
[7] Instituto de Tecnologías en Detección y Astropartículas (CNEA, CONICET, UNSAM), Buenos Aires, Argentina
[8] International Center of Advanced Studies and Instituto de Ciencias Físicas, ECyT-UNSAM and CONICET, Campus Miguelete – San Martín, Buenos Aires, Argentina
[9] Laboratorio Atmósfera – Departamento de Investigaciones en Láseres y sus Aplicaciones – UNIDEF (CITEDEF-CONICET), Argentina
[10] Observatorio Pierre Auger, Malargüe, Argentina
[11] Observatorio Pierre Auger and Comisión Nacional de Energía Atómica, Malargüe, Argentina
[12] Universidad Tecnológica Nacional – Facultad Regional Buenos Aires, Buenos Aires, Argentina
[13] University of Adelaide, Adelaide, S.A., Australia
[14] Université Libre de Bruxelles (ULB), Brussels, Belgium
[15] Vrije Universiteit Brussels, Brussels, Belgium
[16] Centro Federal de Educação Tecnológica Celso Suckow da Fonseca, Petropolis, Brazil
[17] Instituto Federal de Educação, Ciência e Tecnologia do Rio de Janeiro (IFRJ), Brazil
[18] Universidade de São Paulo, Escola de Engenharia de Lorena, Lorena, SP, Brazil
[19] Universidade de São Paulo, Instituto de Física de São Carlos, São Carlos, SP, Brazil
[20] Universidade de São Paulo, Instituto de Física, São Paulo, SP, Brazil
[21] Universidade Estadual de Campinas, IFGW, Campinas, SP, Brazil
[22] Universidade Estadual de Feira de Santana, Feira de Santana, Brazil
[23] Universidade Federal de Campina Grande, Centro de Ciencias e Tecnologia, Campina Grande, Brazil
[24] Universidade Federal do ABC, Santo André, SP, Brazil
[25] Universidade Federal do Paraná, Setor Palotina, Palotina, Brazil
[26] Universidade Federal do Rio de Janeiro, Instituto de Física, Rio de Janeiro, RJ, Brazil
[27] Universidade Federal do Rio de Janeiro (UFRJ), Observatório do Valongo, Rio de Janeiro, RJ, Brazil
[28] Universidade Federal Fluminense, EEIMVR, Volta Redonda, RJ, Brazil
[29] Universidad de Medellín, Medellín, Colombia
[30] Universidad Industrial de Santander, Bucaramanga, Colombia

PoS(ICRC2023)319

[31] Charles University, Faculty of Mathematics and Physics, Institute of Particle and Nuclear Physics, Prague, Czech Republic
[32] Institute of Physics of the Czech Academy of Sciences, Prague, Czech Republic
[33] Palacky University, Olomouc, Czech Republic
[34] CNRS/IN2P3, IJCLab, Université Paris-Saclay, Orsay, France
[35] Laboratoire de Physique Nucléaire et de Hautes Energies (LPNHE), Sorbonne Université, Université de Paris, CNRS-IN2P3, Paris, France
[36] Univ. Grenoble Alpes, CNRS, Grenoble Institute of Engineering Univ. Grenoble Alpes, LPSC-IN2P3, 38000 Grenoble, France
[37] Université Paris-Saclay, CNRS/IN2P3, IJCLab, Orsay, France
[38] Bergische Universität Wuppertal, Department of Physics, Wuppertal, Germany
[39] Karlsruhe Institute of Technology (KIT), Institute for Experimental Particle Physics, Karlsruhe, Germany
[40] Karlsruhe Institute of Technology (KIT), Institut für Prozessdatenverarbeitung und Elektronik, Karlsruhe, Germany
[41] Karlsruhe Institute of Technology (KIT), Institute for Astroparticle Physics, Karlsruhe, Germany
[42] RWTH Aachen University, III. Physikalisches Institut A, Aachen, Germany
[43] Universität Hamburg, II. Institut für Theoretische Physik, Hamburg, Germany
[44] Universität Siegen, Department Physik – Experimentelle Teilchenphysik, Siegen, Germany
[45] Gran Sasso Science Institute, L'Aquila, Italy
[46] INFN Laboratori Nazionali del Gran Sasso, Assergi (L'Aquila), Italy
[47] INFN, Sezione di Catania, Catania, Italy
[48] INFN, Sezione di Lecce, Lecce, Italy
[49] INFN, Sezione di Milano, Milano, Italy
[50] INFN, Sezione di Napoli, Napoli, Italy
[51] INFN, Sezione di Roma "Tor Vergata", Roma, Italy
[52] INFN, Sezione di Torino, Torino, Italy
[53] Istituto di Astrofisica Spaziale e Fisica Cosmica di Palermo (INAF), Palermo, Italy
[54] Osservatorio Astrofisico di Torino (INAF), Torino, Italy
[55] Politecnico di Milano, Dipartimento di Scienze e Tecnologie Aerospaziali , Milano, Italy
[56] Università del Salento, Dipartimento di Matematica e Fisica "E. De Giorgi", Lecce, Italy
[57] Università dell'Aquila, Dipartimento di Scienze Fisiche e Chimiche, L'Aquila, Italy
[58] Università di Catania, Dipartimento di Fisica e Astronomia "Ettore Majorana", Catania, Italy
[59] Università di Milano, Dipartimento di Fisica, Milano, Italy
[60] Università di Napoli "Federico II", Dipartimento di Fisica "Ettore Pancini", Napoli, Italy
[61] Università di Palermo, Dipartimento di Fisica e Chimica "E. Segrè", Palermo, Italy
[62] Università di Roma "Tor Vergata", Dipartimento di Fisica, Roma, Italy
[63] Università Torino, Dipartimento di Fisica, Torino, Italy
[64] Benemérita Universidad Autónoma de Puebla, Puebla, México
[65] Unidad Profesional Interdisciplinaria en Ingeniería y Tecnologías Avanzadas del Instituto Politécnico Nacional (UPIITA-IPN), México, D.F., México
[66] Universidad Autónoma de Chiapas, Tuxtla Gutiérrez, Chiapas, México
[67] Universidad Michoacana de San Nicolás de Hidalgo, Morelia, Michoacán, México
[68] Universidad Nacional Autónoma de México, México, D.F., México
[69] Universidad Nacional de San Agustin de Arequipa, Facultad de Ciencias Naturales y Formales, Arequipa, Peru
[70] Institute of Nuclear Physics PAN, Krakow, Poland
[71] University of Łódź, Faculty of High-Energy Astrophysics,Łódź, Poland
[72] Laboratório de Instrumentação e Física Experimental de Partículas – LIP and Instituto Superior Técnico – IST, Universidade de Lisboa – UL, Lisboa, Portugal
[73] "Horia Hulubei" National Institute for Physics and Nuclear Engineering, Bucharest-Magurele, Romania
[74] Institute of Space Science, Bucharest-Magurele, Romania
[75] University Politehnica of Bucharest, Bucharest, Romania
[76] Center for Astrophysics and Cosmology (CAC), University of Nova Gorica, Nova Gorica, Slovenia
[77] Experimental Particle Physics Department, J. Stefan Institute, Ljubljana, Slovenia

PoS(ICRC2023)319

[78] Universidad de Granada and C.A.F.P.E., Granada, Spain
[79] Instituto Galego de Física de Altas Enerxías (IGFAE), Universidade de Santiago de Compostela, Santiago de Compostela, Spain
[80] IMAPP, Radboud University Nijmegen, Nijmegen, The Netherlands
[81] Nationaal Instituut voor Kernfysica en Hoge Energie Fysica (NIKHEF), Science Park, Amsterdam, The Netherlands
[82] Stichting Astronomisch Onderzoek in Nederland (ASTRON), Dwingeloo, The Netherlands
[83] Universiteit van Amsterdam, Faculty of Science, Amsterdam, The Netherlands
[84] Case Western Reserve University, Cleveland, OH, USA
[85] Colorado School of Mines, Golden, CO, USA
[86] Department of Physics and Astronomy, Lehman College, City University of New York, Bronx, NY, USA
[87] Michigan Technological University, Houghton, MI, USA
[88] New York University, New York, NY, USA
[89] University of Chicago, Enrico Fermi Institute, Chicago, IL, USA
[90] University of Delaware, Department of Physics and Astronomy, Bartol Research Institute, Newark, DE, USA
[91] University of Wisconsin-Madison, Department of Physics and WIPAC, Madison, WI, USA

—

[a] Louisiana State University, Baton Rouge, LA, USA
[b] also at University of Bucharest, Physics Department, Bucharest, Romania
[c] School of Physics and Astronomy, University of Leeds, Leeds, United Kingdom
[d] now at Agenzia Spaziale Italiana (ASI). Via del Politecnico 00133, Roma, Italy
[e] Fermi National Accelerator Laboratory, Fermilab, Batavia, IL, USA
[f] now at Graduate School of Science, Osaka Metropolitan University, Osaka, Japan
[g] now at ECAP, Erlangen, Germany
[h] Max-Planck-Institut für Radioastronomie, Bonn, Germany
[i] also at Kapteyn Institute, University of Groningen, Groningen, The Netherlands
[j] Colorado State University, Fort Collins, CO, USA
[k] Pennsylvania State University, University Park, PA, USA

Acknowledgments

The successful installation, commissioning, and operation of the Pierre Auger Observatory would not have been possible without the strong commitment and effort from the technical and administrative staff in Malargüe. We are very grateful to the following agencies and organizations for financial support:

Argentina – Comisión Nacional de Energía Atómica; Agencia Nacional de Promoción Científica y Tecnológica (ANPCyT); Consejo Nacional de Investigaciones Científicas y Técnicas (CONICET); Gobierno de la Provincia de Mendoza; Municipalidad de Malargüe; NDM Holdings and Valle Las Leñas; in gratitude for their continuing cooperation over land access; Australia – the Australian Research Council; Belgium – Fonds de la Recherche Scientifique (FNRS); Research Foundation Flanders (FWO); Brazil – Conselho Nacional de Desenvolvimento Científico e Tecnológico (CNPq); Financiadora de Estudos e Projetos (FINEP); Fundação de Amparo à Pesquisa do Estado de Rio de Janeiro (FAPERJ); São Paulo Research Foundation (FAPESP) Grants No. 2019/10151-2, No. 2010/07359-6 and No. 1999/05404-3; Ministério da Ciência, Tecnologia, Inovações e Comunicações (MCTIC); Czech Republic – Grant No. MSMT CR LTT18004, LM2015038, LM2018102, CZ.02.1.01/0.0/0.0/16_013/0001402, CZ.02.1.01/0.0/0.0/18_046/0016010 and CZ.02.1.01/0.0/0.0/17_049/0008422; France – Centre de Calcul IN2P3/CNRS; Centre National de la Recherche Scientifique (CNRS); Conseil Régional Ile-de-France; Département Physique Nucléaire et Corpusculaire (PNC-IN2P3/CNRS); Département Sciences de l'Univers (SDU-INSU/CNRS); Institut Lagrange de Paris (ILP) Grant No. LABEX ANR-10-LABX-63 within the Investissements d'Avenir Programme Grant No. ANR-11-IDEX-0004-02; Germany – Bundesministerium für Bildung und Forschung (BMBF); Deutsche Forschungsgemeinschaft (DFG); Finanzministerium Baden-Württemberg; Helmholtz Alliance for Astroparticle Physics (HAP); Helmholtz-Gemeinschaft Deutscher Forschungszentren (HGF); Ministerium für Kultur und Wissenschaft des Landes Nordrhein-Westfalen; Ministerium für Wissenschaft, Forschung und Kunst des Landes Baden-Württemberg; Italy – Istituto Nazionale di Fisica Nucleare (INFN); Istituto Nazionale di Astrofisica (INAF); Ministero dell'Universitá e della Ricerca (MUR); CETEMPS Center of Excellence; Ministero degli Affari Esteri (MAE), ICSC Centro Nazionale di Ricerca in High Performance Computing, Big Data

and Quantum Computing, funded by European Union NextGenerationEU, reference code CN_00000013; México – Consejo Nacional de Ciencia y Tecnología (CONACYT) No. 167733; Universidad Nacional Autónoma de México (UNAM); PAPIIT DGAPA-UNAM; The Netherlands – Ministry of Education, Culture and Science; Netherlands Organisation for Scientific Research (NWO); Dutch national e-infrastructure with the support of SURF Cooperative; Poland – Ministry of Education and Science, grants No. DIR/WK/2018/11 and 2022/WK/12; National Science Centre, grants No. 2016/22/M/ST9/00198, 2016/23/B/ST9/01635, 2020/39/B/ST9/01398, and 2022/45/B/ST9/02163; Portugal – Portuguese national funds and FEDER funds within Programa Operacional Factores de Competitividade through Fundação para a Ciência e a Tecnologia (COMPETE); Romania – Ministry of Research, Innovation and Digitization, CNCS-UEFISCDI, contract no. 30N/2023 under Romanian National Core Program LAPLAS VII, grant no. PN 23 21 01 02 and project number PN-III-P1-1.1-TE-2021-0924/TE57/2022, within PNCDI III; Slovenia – Slovenian Research Agency, grants P1-0031, P1-0385, I0-0033, N1-0111; Spain – Ministerio de Economía, Industria y Competitividad (FPA2017-85114-P and PID2019-104676GB-C32), Xunta de Galicia (ED431C 2017/07), Junta de Andalucía (SOMM17/6104/UGR, P18-FR-4314) Feder Funds, RENATA Red Nacional Temática de Astropartículas (FPA2015-68783-REDT) and María de Maeztu Unit of Excellence (MDM-2016-0692); USA – Department of Energy, Contracts No. DE-AC02-07CH11359, No. DE-FR02-04ER41300, No. DE-FG02-99ER41107 and No. DE-SC0011689; National Science Foundation, Grant No. 0450696; The Grainger Foundation; Marie Curie-IRSES/EPLANET; European Particle Physics Latin American Network; and UNESCO.